MASSACHUSETTS INSTITUTE OF TECHNOLOGY

PLASMA FUSION CENTER

ASSOCIATED WITH

DEPARTMENT OF AERONAUTICS AND ASTRONAUTICS
DEPARTMENT OF ELECTRICAL ENGINEERING
AND COMPUTER SCIENCE
DEPARTMENT OF MATERIALS SCIENCE
AND ENGINEERING
DEPARTMENT OF MECHANICAL ENGINEERING
DEPARTMENT OF NUCLEAR ENGINEERING
DEPARTMENT OF PHYSICS
FRANCIS BITTER NATIONAL MAGNET LABORATORY
RESEARCH LABORATORY OF ELECTRONICS

This work was supported by the U.S. Department of Energy Contract No. DE-AC02-78ET51013. Reproduction, translation, publication, use and disposal, in whole or part, by or for the United States government is permitted.

DISCLAIMER

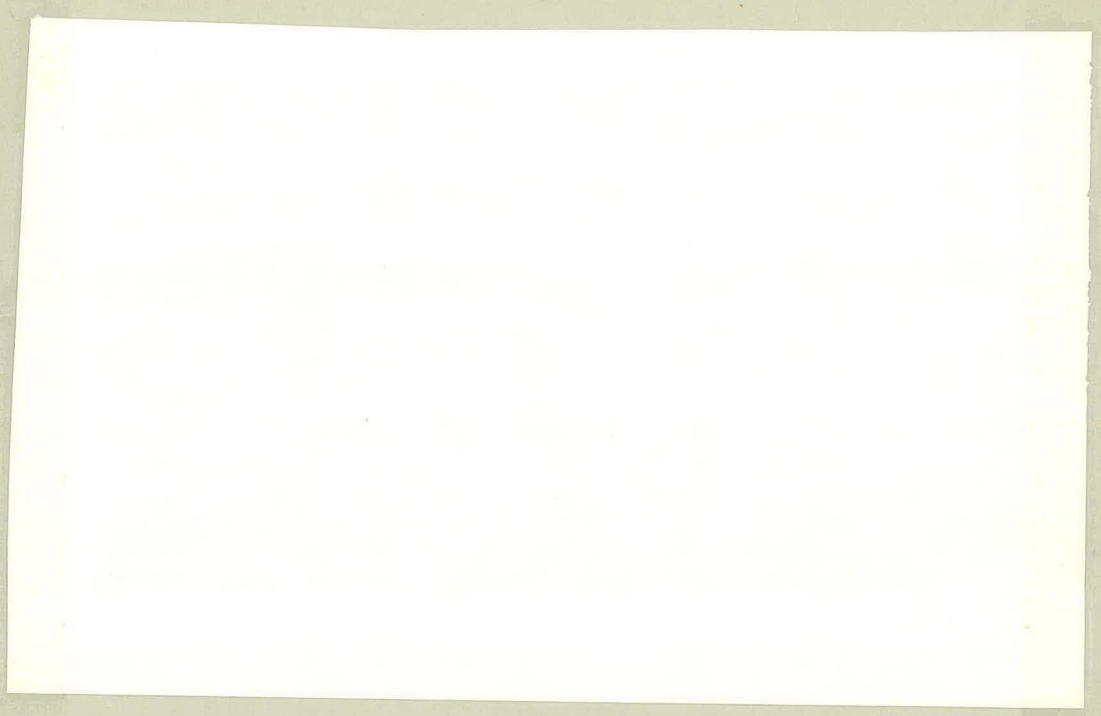

Printed in the United States of America

Available from:

National Technical Information Service
U.S. Department of Commerce
5285 Port Royal Road
Springfield, VA 22161

DOMESTIC PRICE CODES

Standard Priced Documents (Schedule A)

Effective January 1, 1982

Prices are for customers in the United States, Canada, and Mexico.

Code	Price	Page Range	Code	Price	Page Range
A01	$ 4.00	Microfiche	A13	$22.50	276 - 300
A02	6.00	001 - 025	A14	24.00	301 - 325
A03	7.50	026 - 050	A15	25.50	326 - 350
A04	9.00	051 - 075	A16	27.00	351 - 375
A05	10.50	076 - 100	A17	28.50	376 - 400
A06	12.00	101 - 125	A18	30.00	401 - 425
A07	13.50	126 - 150	A19	31.50	426 - 450
A08	15.00	151 - 175	A20	33.00	451 - 475
A09	16.50	176 - 200	A21	34.50	476 - 500
A10	18.00	201 - 225	A22	36.00	501 - 525
A11	19.50	226 - 250	A23	37.50	526 - 550
A12	21.00	251 - 275	A24	39.00	551 - 575
			A25	40.50	576 - 600

For documents over 600 pages, add $1.50 for each additional 25-page increment.

A99--Contact NTIS for a price quote.

CONF-820345--10

DOE/ET/51013--41

DE82 013674

PFC/CP-82-5 DOE/ET/51013-41 UC20F

LOWER-HYBRID-HEATING EXPERIMENTS ON THE ALCATOR C AND THE VERSATOR II TOKAMAKS*

Alcator C Group

M. Porkolab, J. J. Schuss, Y. Takase, S. Texter, C. L. Fiore, R. Gandy, M. J. Greenwald, D. A. Gwinn, B. Lipschultz, E. S. Marmar, D. S. Pappas, R. R. Parker, J. E. Rice, J. L. Terry, S. M. Wolfe

Versator II Group

S. F. Knowlton, K. I. Chen, S. C. Luckhardt, M. J. Mayberry, M. Porkolab

Theory Group

P. I. Bonoli, B. Coppi, R. Englade

Plasma Fusion Center
Massachusetts Institute of Technology
Cambridge, Massachusetts 02139 USA

*Invited paper presented at the "Third International Symposium on Heating in Toroidal Devices", March 22, 1982.

LOWER HYBRID HEATING EXPERIMENTS ON THE ALCATOR C AND THE VERSATOR II TOKAMAKS

Alcator C Group

M. Porkolab, J. J. Schuss, Y. Takase, S. Texter, C. L. Fiore, R. Gandy, M. J. Greenwald, D. A. Gwinn, B. Lipschultz, E. S. Marmar, D. S. Pappas, R. R. Parker, J. E. Rice, J. L. Terry, S. M. Wolfe

Versator II Group

S. F. Knowlton, K. I. Chen, S. C. Luckhardt, M. J. Mayberry, M. Porkolab

Theory Group

P. I. Bonoli, B. Coppi, R. Englade

Plasma Fusion Center
Massachusetts Institute of Technology
Cambridge, Massachusetts 02139 USA

ABSTRACT

We report on initial results from lower hybrid wave heating experiments carried out on the MIT Alcator C and Versator II tokamaks. In the Alcator C experiments a 4 waveguide array, with internally brazed ceramic windows has been used to inject 160 kW of microwave power at 4.6 GHz into the plasma with $n_o \leq 1 \times 10^{15}$ cm^{-3}, and $B_o \leq 12$ T. An RF power density of 8 kW/cm^2 has been transmitted into the plasma without RF breakdown. RF coupling studies show optimal coupling ($R \leq 10\%$) when the local density at the waveguide mouth is 25-50 times overdense. Initial heating experiments show an ion tail formation in hydrogen discharge peaking at a density of $\bar{n} \simeq 2.7 \times 10^{14}$ cm^{-3} at $B = 8.9$ T, and bulk ion heating at a density of $\bar{n} \simeq 1.5 \times 10^{14}$ cm^{-3} at $B \simeq 11$ T. Evidence of RF current enhancement has been observed at a density of $n \simeq 3 \times 10^{13}$ cm^{-3}.

In the Versator II tokamak initial ion heating studies have been carried out using an 800 MHz, 140 kW klystron. With 50 kW of net RF power injected through a 4 waveguide grill at $B = 1.3$ T and $\bar{n} = 2.5 \times 10^{13}$ cm^{-3}, Doppler broadening of the OVII and NVI lines shows a $\Delta T_i = 50$ eV rise in the bulk ion temperature. A significant RF produced ion tail is also observed by charge exchange analysis.

We have succeeded in combining a toroidal ray-tracing code and a 1-D transport code to study the heating density bands and heating efficiencies. Results related to the foregoing experiments are presented. We find that collisional absorption of rays in the outer cold plasma regions may significantly affect the lower hybrid wave heating efficiency.

ALCATOR C EXPERIMENTS

1. RF Power System and Antenna

We have begun a series of lower hybrid heating and current drive experiments in the MIT Alcator C tokamak [1]. The operating frequency of the Varian built cw klystrons is 4.6 GHz, and the pulse length (determined by power supply capabilities) is 0.5 sec at the full power rating of 250 kW per klystron. The complete system will consist of 16 klystrons, for a total power of 4.0 MW at the source. The system is divided into four subsystems, each consisting of a power supply-modulator unit which powers four klystrons. The relative phase of each klystron is electronically adjustable, and each klystron feeds one column of a 4 X 4 array of waveguides. The waveguides have internally brazed ceramic (BeO) vacuum windows located 10-12 cm from the plasma end. The fabrication of the first of these units has just been completed by Varian Associates and delivered to MIT.

In the present paper we summarize initial RF coupling and heating results obtained by a 1 X 4 waveguide array which served as a prototype for the antenna development program. The dimensions of the 304-L stainless steel waveguides are 0.9 X 5.75 cm, with 0.2 cm wall separation. This waveguide array produces a Brambilla spectrum which peaks at $N_{\parallel} \simeq 3$, and it extends from $N_{\parallel} = 2$ to 4, when the relative phasing of adjacent waveguides is $(0,\pi,0,\pi)$ radians. In this coupler the ceramic windows were placed approximately 16 cm from the waveguide mouth at the plasma end. The waveguide array is movable by a bellows assembly so that the RF coupling to the plasma could be optimized. After proper cleaning and thermal cycling a small leak developed in one of the waveguides (near the window). In order to reduce nitrogen leakage into the vacuum chamber, a back-up mica window was installed in each waveguide and the space between the mica and ceramic windows was evacuated. Eight to ten seconds prior to RF injection into the plasma a nitrogen gas pulse at a fill pressure of $p \sim 250$ torr was injected into the waveguides between the windows. Under optimal conditions such techniques allowed us to inject up to 8 kW/cm^2 RF power density into the plasma (or a total maximum power of $P \sim 160$ kW) for 50 msec without evidence of RF breakdown or plasma formation in the waveguides. In vacuum RF powers in excess of 200 kW were transmitted through the array.

On top of the waveguide array an RF and/or Langmuir probe array (two probes) was installed which could be moved in front of the waveguides. Thus the local plasma conditions (density and temperature) as well as the RF fields (pump wave and parametric decay spectra) could be monitored during these experiments.

2. RF Coupling Experiments

Before starting the high power experiments, by moving the waveguide array radially we studied the RF coupling between the array and the plasma at low power. In Fig. 1 we display the reflection coefficient R as a function of density at the waveguide mouth. In these data the relative waveguide phasing was $(0,\pi,0,\pi)$, and an optimum coupling position of $r = 17.8$ cm was obtained. These experiments were carried out at low RF power ($P \simeq 1$ Watt) so as to stay within the limits of linear theory. We see that the minimum reflection coefficient of $R \simeq 5$-10% is obtained when the density at the waveguide mouth is highly overdense ($n_{WGD}/n_{crit} \simeq 25$-50) where $n_{crit} \simeq 2.6 \times 10^{11}$ cm^{-3}. In the

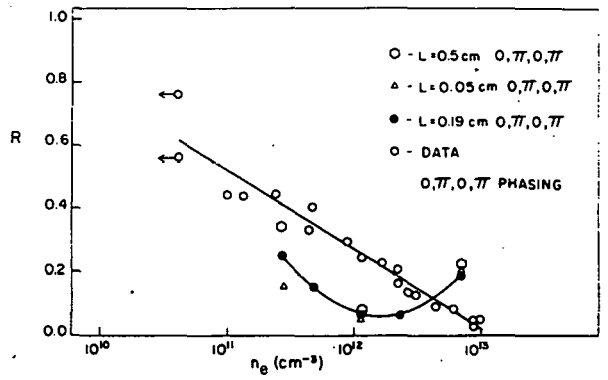

Fig. 1. Global waveguide array reflectivity R vs. n_e at the waveguide mouth for all waveguide positions and for a relative waveguide phasing of $0,\pi,0,\pi$. The curves are the theoretically predicted R for the same n_e and for L = 0.5 cm, 0.05 cm, and 0.19 cm.

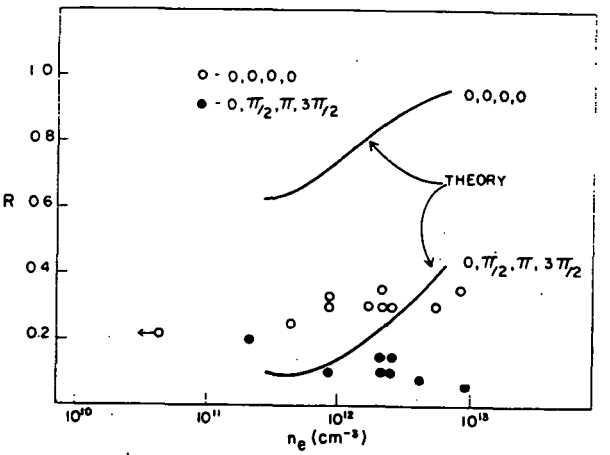

Fig. 2. Global waveguide array reflectivity R vs. n_e at the waveguide mouth for all waveguide positions and for relative phasings of 0 and $\pi/2$. The curves are the theoretical predictions for the same conditions.

same figure we also show the theoretically calculated reflection coefficients using a modified Brambilla code which assumes a step density at the waveguide mouth [2,3]. Here we used three different values of the density gradient at the waveguide mouth, L, which covers the range of values measured in these experiments with a Langmuir probe. We see that while qualitative similarities exist, quantitative agreement between experiment and theory is not possible. This is especially true when the four waveguides were in phase or only 90° out of phase, as shown in Fig. 2. The cause of this disagreement at present is not understood. It is interesting to note from Fig. 1 that the straight-line behavior of R versus n_{WGD}, the density at the waveguide mouth is independent of density gradients.

We have also carried out high power ($P/A = 8$ kW/cm^2) coupling experiments. Using the a = 16.5 cm Alcator C plasma column, we found no significant differences from the low power experiments. This may be understood by noting that even at these high power experiments $E_z^2/8\pi nT \sim 0.1$ at the waveguide mouth (where $n_{WGD} \simeq 10^{13}$ cm^{-3}, $T_{WGD} \simeq 3$ eV, and $E_z \simeq 3$ kV/cm) and thus ponderomotive forces are not expected to play a significant role here.

3. Heating Experiments

Because Alcator C operates in a wide variety of modes, we can consider several heating regimes. In particular, at the lowest densities, $\bar{n} \lesssim 5 \times 10^{13}$ cm^{-3}, we may expect to see current drive, and at intermediate densities $\bar{n} \simeq (1\text{-}2) \times 10^{14}$ cm^{-3}, we expect to see electron heating (and bulk ion heating by collisional equilibration). At higher densities ($\bar{n} \simeq (2.5\text{-}4) \times 10^{14}$ cm^{-3} in H_2 at $B \gtrsim 8$ T and/or $\bar{n} \simeq 8 \times 10^{14}\text{-}1.5 \times 10^{15}$ cm^{-3} in D_2 at $B \gtrsim 12$ T) we expect to see ion heating in front of the linear mode-conversion layer. These estimates assume that the initial ohmic heating produces $T_e \simeq T_i \gtrsim 1$ keV at the higher densities, $T_e \simeq 2$ keV at the intermediate densities, and that a non-Maxwellian tail develops at the low density current drive regime. We

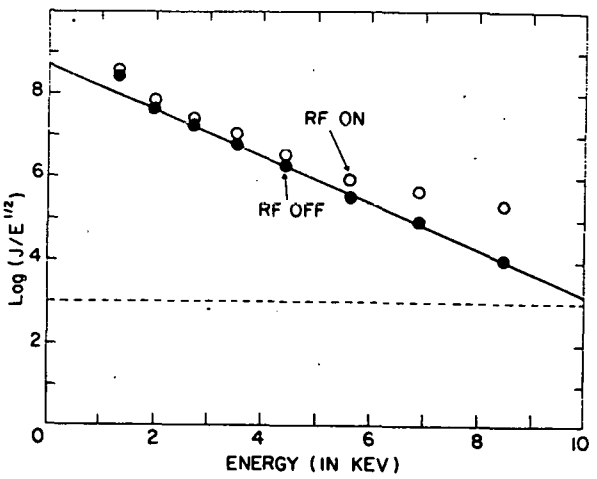

Fig. 3. Charge exchange neutral spectrum for $\bar{n}_e \tilde{\sim} 3 \times 10^{14}$ cm^{-3}, $B_T = 8.9$ T, and $P_{RF} = 110$ kW in hydrogen discharge.

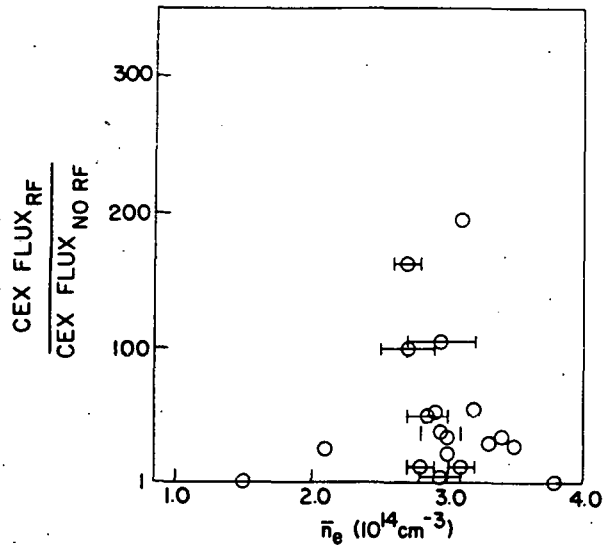

Fig. 4. 10 keV hydrogen neutral flux enhancement during RF injection vs. $\bar{n}_e$ for $P_{RF} = 100$ kW and $B_T = 8.9$ T.

believe we have observed experimentally all three regimes. The exact density bands may well be modified by toroidal effects[4].

Because Alcator C was operating in the past five months with two different limiter sizes, namely a 16.5 cm limiter and a 10 cm limiter, and since the RF/ohmic heating power balance is better with the 10 cm limiter, we shall present here heating results obtained only with the 10 cm limiter plasma. We note that at the higher densities the 10 cm limiter plasma is more preferable for RF heating experiments since the density profile is more peaked ($n_o/\bar{n} \simeq 1.5$) than the 16.5 cm plasma ($n_o/\bar{n} \simeq 1.3$). However, for the low density current drive experiments we used the 16.5 cm plasma.

A. Ion Tail Formation

When we operate in a hydrogen plasma at a density of $\bar{n} \simeq (3\text{-}4) \times 10^{14}$cm^{-3} at $B \gtrsim 8$ T, according to quasi-linear theory, we expect to see ion tail formation, and concomitant bulk ion heating due to thermalization of this ion tail if it is well confined. In Fig. 3 we show charge exchange spectra obtained in this density range with and without RF power. The spectrum with RF shows the formation of an ion tail extending out to at least 10 keV.

In Fig. 4 we show the variation of the 10 keV charge exchange flux as a function of density. We see that the ion tail production peaks at a density of $\bar{n} \simeq 2.7 \times 10^{14}$ cm^{-3}, and it exists in a range $\bar{n} \simeq (2.2\text{-}3.5) \times 10^{14}$ cm^{-3}. The ion tail is believed to originate near the central region of the plasma column. This was ascertained by a vertical scan with the charge exchange detector, which showed that the RF induced enhancement of neutral flux decreased as the detector scanned downward below the plasma center. At the present RF power levels we cannot determine the exact amount of power deposited into this ion tail, or if there is significant bulk ion heating due to this tail. On the 16.5 cm radius plasma at similar densities this ion tail was not observed.

We have also carried out experiments by injecting 5% D_2 gas so as to observe neutron production in case a deuterium tail formed. We found no observable enhancement of neutron production from the minority deuterons. We conclude that the ion tail consisted of protons only. This is in agreement with recent calculations of lower hybrid quasi-linear ion tail production in a multiple species plasma where it was found that all the power was absorbed by the lighter species in such a plasma [5]. Finally, we note that the ion tail was formed only when the relative waveguide phasing was 180° or 90°, but not when it was 0°.

The observation of the fast hydrogen ion tail is consistent with strong damping of lower hybrid waves having $N_{\parallel} \simeq 4$ in the plasma core. Linear damping theory predicts the lack of absorption of waves having $N_{\parallel} \simeq 3$ at these plasma parameters. Since waveguide plasma coupling theory shows that the wave power spectrum emitted by the waveguide grill is peaked at $N_{\parallel} = 3$, it would seem that a mild upshift in $N_{\parallel}$ of the lower hybrid waves as they penetrate the plasma would be required to explain the ion tail. Figure 5 shows the prediction of quasi-linear theory [6] for the fast ion distribution function for the experimental conditions of ion tail formation ($n_{eo} = 1.6\ \bar{n}_e = 4.8 \times 10^{14}$ cm^{-3}, $B_T = 8.9$ T, $T_i = 750$ eV). Curve 1 shows $f(E_{\perp})$ for a spectrum of waves with $N_{\parallel} = 3.75 \pm 0.25$ and $E = 2.2$ kV/cm. Eighty percent of the RF power incident on the central plasma core ($r = 3$ cm) would be absorbed. Curve 2 graphs $f(E_{\perp})$ for a spectrum in the range $N_{\parallel} = 3 \pm 0.25$. Here there is no significant ion tail or absorption. Curve 3 graphs $f(E_{\perp})$ for a wave spectrum comprised of $N_{\parallel}$ components from 2 to 4, with the peak being at $N_{\parallel} = 3$ (similar to that launched by the Alcator C waveguide array). Strong absorption and fast ion tail formation reappear, as the higher values of $N_{\parallel}$ kick up ions to energies where they continue to damp on the lower $N_{\parallel}$'s. Thus the inclusion of quasi-linear theory only requires the presence of some wave power at $N_{\parallel} \gtrsim 3.5$ (which is consistent with our waveguide spectrum). Furthermore, toroidal effects could also upshift our spectrum, which could also account for the observed ion tail formation (and possibly bulk ion heating) in these experiments.

B. Electron Heating Regime

These experiments were carried out in the regime of $\bar{n} \simeq (1\text{-}2) \times 10^{14}$ cm^{-3} in 10 cm radius deuterium plasma at a magnetic field of $B \simeq 11$ T. Typical ohmic heating powers were 400 kW ($I = 200$ kAmp, $V_L \simeq 2$ Volt) which produced $T_e \simeq 1.7$ keV, $T_i \simeq 1.1$ keV. Evidence of electron heating was observed throughout this regime for a net transmitted RF power in the range of $P_{RF} \simeq 70\text{-}110$kW. Higher powers were not easy to transmit since the curvature of the waveguide array was designed for a 17 cm plasma and in the 10 cm plasma the density decreased vertically in front of the lower half of the waveguide array to non-optimal values. Nevertheless, the RF to ohmic power balance was still better in this plasma than in the 16.5 cm plasma.

Evidence of electron heating was observed on the soft X-ray emission and on the $2\omega_{ce}$ emission. Unfortunately, both of these diagnostics are sensitive to electron tail formation, and the exact bulk electron temperature increase was not ascertained. (The Thomson scattering apparatus was not operating during these experiments.) Hence, we deduced the occurence of bulk electron heating from the increase in ion temperature caused by collisional eqilibration between electrons and ions. Such effects are not sensitive to the existence of an electron tail (which slows down by collisions on bulk electrons). Furthermore, a density of $\bar{n} \simeq 1.5 \times 10^{14}$ cm^{-3} in deuterium at

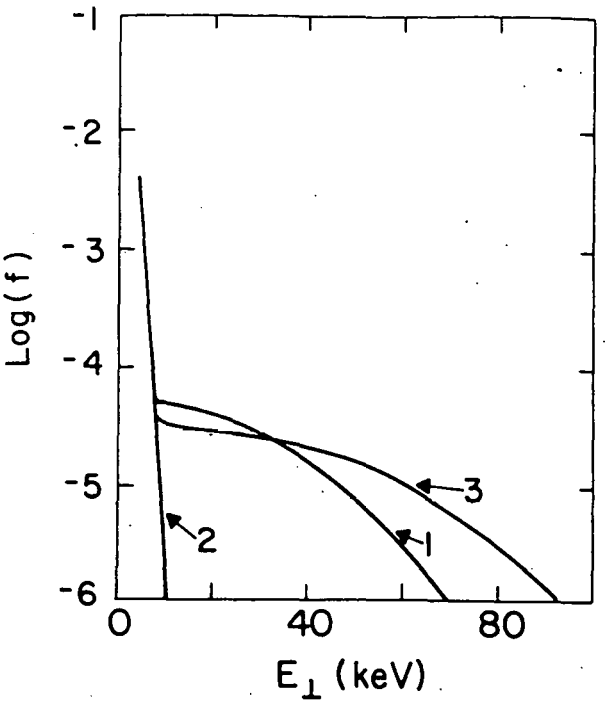

Fig. 5. Graph of hydrogen ion distribution function f vs. $E_\perp$ calculated using quasi-linear theory, $n_e = 4.8 \times 10^{14}$ cm^{-3}, $B_T = 8.9$ T, and $T_i = 0.75$ keV. Curve 1: $n_{\parallel max} = 4$, $n_{\parallel min} = 3.5$, Curve 2: $n_{\parallel max} = 3.25$, $n_{\parallel min} = 2.75$, Curve 3: $n_{\parallel max} = 4$, $n_{\parallel min} = 2$. In both cases 1 and 3 the lower hybrid wave is strongly damped.

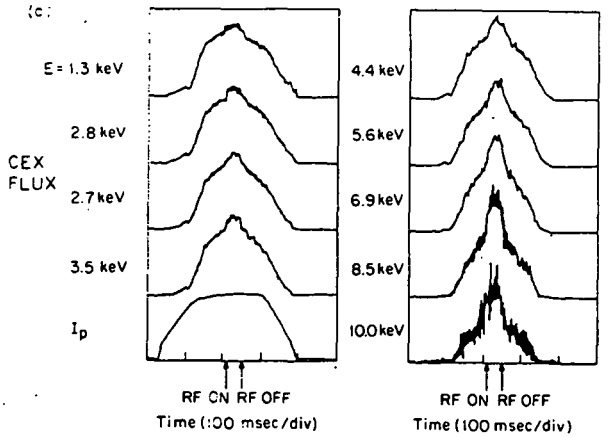

Fig. 6. Averages of charge exchange flux vs. time for several similar shots including RF injection as indicated. Deuterium plasmas, $B_T = 11$ T, $\bar{n}_e \simeq 1.7 \times 10^{14}$ and $P_{RF} = 55$-90 kW.

B = 11 T is an order of magnitude lower than that required for mode-conversion, so direct ion heating is ruled out. We also note that there is a time lag between the initiation of the RF pulse and the rise of the ion temperature which is consistent with the electron ion equilibration time. Thus, we believe that ion heating in this regime is possible only by collisional equilibration from bulk electrons [7].

In Fig. 6 we show evidence of enhanced charge exchange signals during RF injection on various energy channels in the 1.3-10.0 keV range. When analyzed, we find bulk ion temperature increases of the order of $\Delta T_i \simeq 35$-50 eV. We also find that the decay time of the medium to lower energy signals is slow, of the order of 5-10 msec, which is of the order of the bulk ion energy confinement time. In Fig. 7 we show the time variation of the bulk ion temperature rise obtained from the slope of the CX spectrum, averaged over several shots at a density of $\bar{n} \simeq 1.7 \times 10^{14}$ cm^{-3}. The charge exchange spectrum showed no evidence of any ion tail in this case. In Fig. 7 a net rise in the ion temperature of 35-40 eV is observed.

Additionally, a temperature rise of the same magnitude was inferred by an increase in the neutron deduced ion temperature. Evidence of this is presented in Fig. 8 where we see a 20% rise in the neutron flux during RF injection, indicating a 4% rise in the ion temperature (i.e., $\Delta T_i \simeq 40$ eV). Furthermore, we see that the decay time of the neutron signal is of the order of 15 msec, which is of the order of the ion energy confinement time. If the neutrons had been

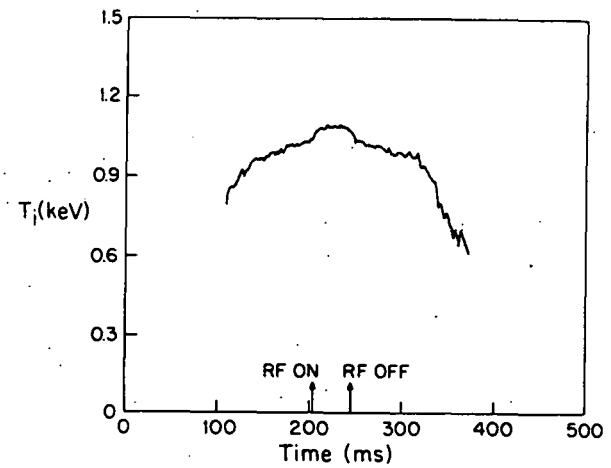

Fig. 7. T_i vs. time deduced from averages of charge exchange flux of several deuterium shots taken both with and without RF; B_T = 11 T, $\bar{n}_e \simeq 1.7 \times 10^{14}$ cm^{-3}, $P_{RF} \simeq$ 55-90 kW.

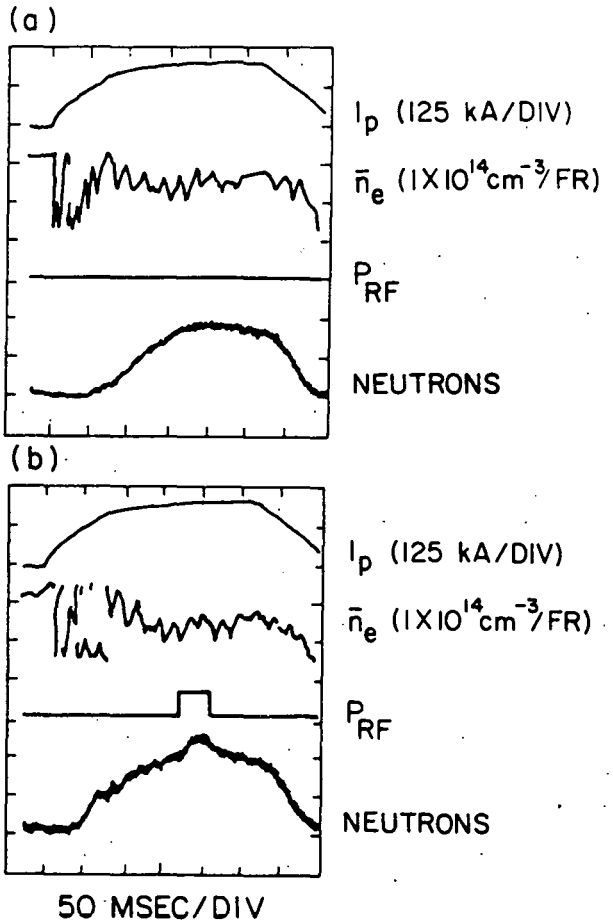

Fig. 8. Typical RF shot in the 10 cm radius deuterium plasma in the electron heating mode; B_T = 11 T and P_{RF} = 70 kW. (a) no RF applied; (b) RF on, showing neutron enhancement.

produced by an ion tail, the neutron decay time should be or the order of a few milli-seconds (not more than 3 msec), as determined by collisional relaxation on ions (E_i < 50 keV) and on electrons ($E_i \gtrsim$ 50 keV) [5]. Thus, the present data clearly indicates bulk ion heating.

These results have been modeled by a combined toroidal ray-tracing 1-D transport code which is described in some detail in Section C in this paper. In Fig. 9 we show the results of such a code for the present parameters. We see that at a density of $\bar{n} = 1.7 \times 10^{14}$ cm^{-3}, D^+ ions and for 100 kW net RF power, the ion temperature rises by ΔT_i = 60 eV, and the electron temperature rises by ΔT_e = 300 eV. Since in the present experiments the typical average injected power was P $\simeq$ 70 kW, we would expect $\Delta T_i \simeq$ 40 eV and $\Delta T_e \simeq$ 200 eV. Thus, the ion temperature rise is in good agreement with the observed value. As shown in Fig. 10, the efficiency needed to get such temperature rises is of the order of 80-90%, and the RF power is deposited in the center of the plasma column by electron (quasi-linear) Landau damping. Collisional absorption near the edge accounts at most for 10% of the incident power. Although we do not

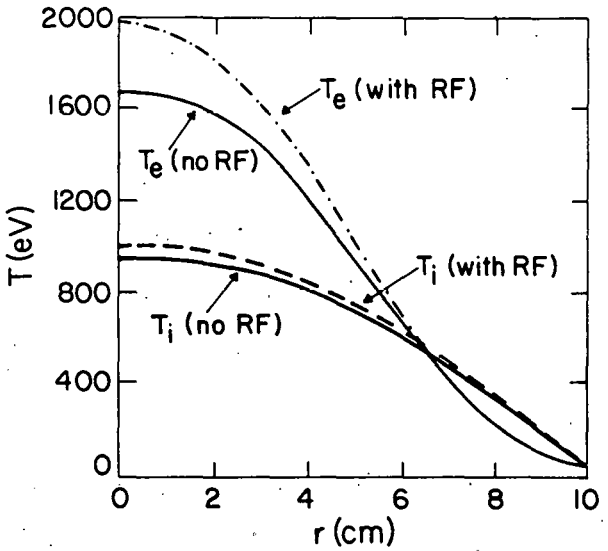

Fig. 9. Transport code modeling of the 10cm radius Alcator C deuterium plasma. B = 10 T, I = 200 kA, $\bar{n}$ = 1.7 X 10^{14} cm^{-3}, P_{RF} = 100 kW.

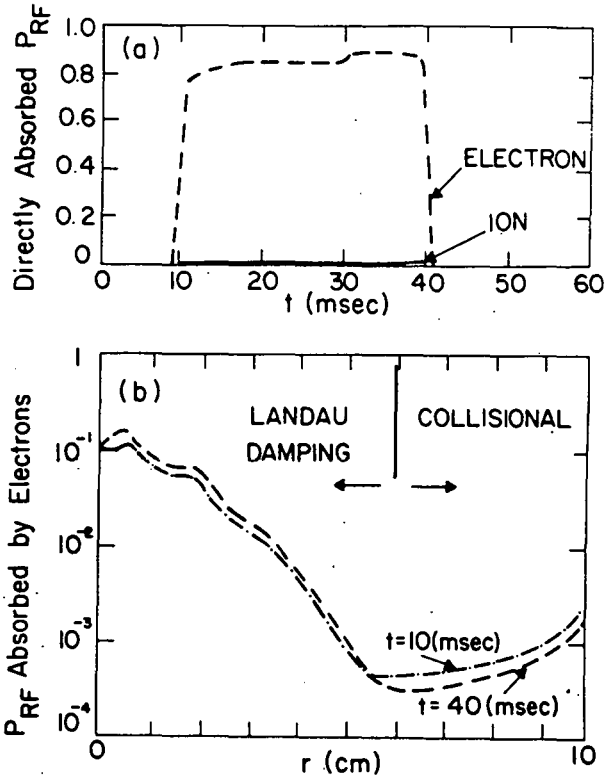

Fig. 10. Transport code modeling of the 10cm radius Alcator C plasma. Parameters as given in Fig. 9. (a) RF power absorbed directly by electrons and ions vs. time; (b) P_{RF} absorbed by electrons vs. r.

have direct measurements of the electron temperature rise, since the ion temperature rise is about the same in the experiment as in the computer code, we expect similar overall efficiency. Finally, we note that these results again depended on waveguide phasing. In particular, we saw evidence of increased wave-electron tail interaction when the waveguides were phased relatively by 90° so that the waves were launched in the direction of ohmic electron drift (as evidenced by increased $2\omega_{ce}$ emission and reduced ion heating efficiency).

C. Current Drive Experiments

Generation of toroidal currents by means of injecting RF power preferentially in a given toroidal direction has been investigated actively both in theory and in experiment [8-12]. Lower hybrid wave injection, in particular, shows promise as an efficient means of adding parallel momentum to electrons, thereby efficiently generating toroidal currents. With the exception of Alcator C, RF current generation in the lower hybrid range of frequencies has been restricted to very low densities, namely $\bar{n} < 10^{13}$ cm^{-3}. On the other hand, in Alcator C we reported observation of LHRF enhanced toroidal currents and associated drop in loop voltage at densities $\bar{n} \simeq 3 \times 10^{13}$ cm^{-3} [3]. In Fig. 11 we present observations of RF induced "current maintenance". These discharges were unlike normal Alcator C discharges in that the plasma current was allowed to decay inductively after the initial current rise. In particular, in Fig. 11(b) we see that the ohmic heating current begins to inductively decay after t = 120 msec into the discharge and then terminates after 240 msec.

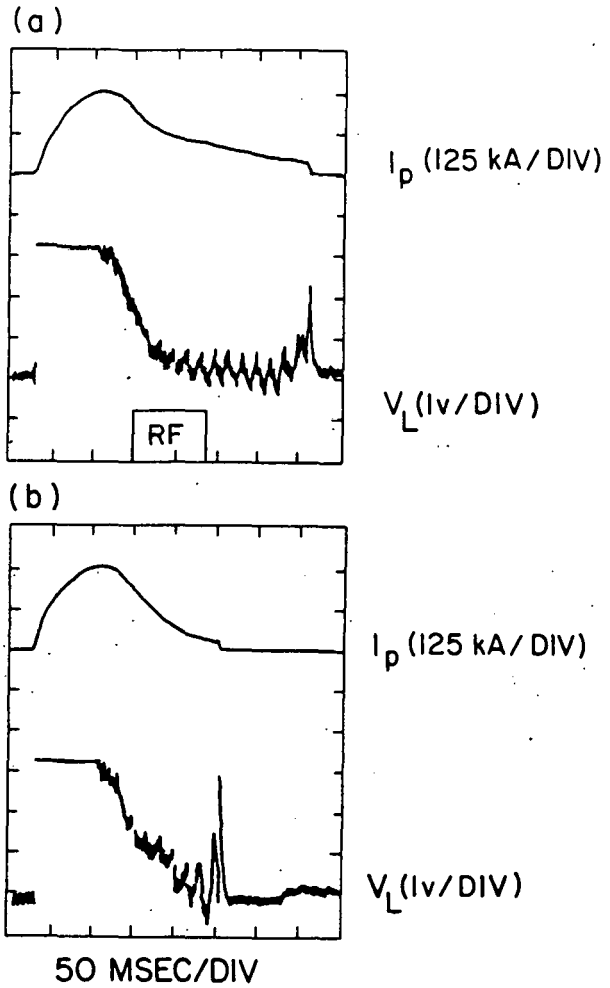

Fig. 11. I_p and V_L vs. time. Hydrogen plasma, B_T = 8T, a_{lim} = 16.5 cm, P_{RF} = 50 kW, and relative waveguide phasing of $0,\pi/2,\pi,3\pi/2$ (wave launcing in the direction of electron drift) (a) RF pulse initiated at t = 120 msec and terminated at t = 200 msec (b) no RF pulse.

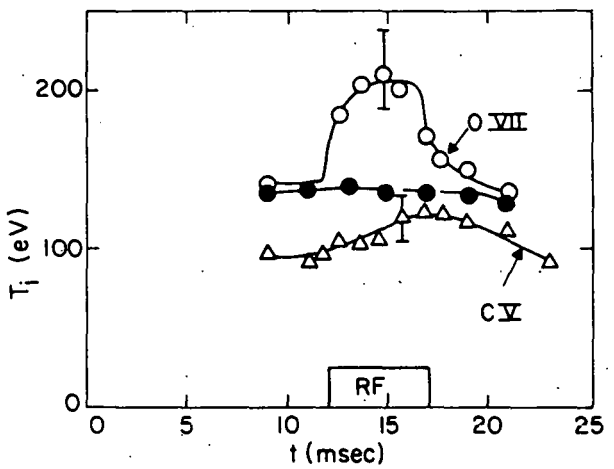

Fig. 12. T_i vs. time deduced from Doppler broadening of the OVII impurity lines (open circles) and the CV line (open triangles). The solid circles denote the OVII lines without RF. $\bar{n}_e$ = 2.6 X 10^{13} cm^{-3}, B_o = 1.35 T, P_{RF} (NET) = 50 kW.

In contrast, as shown in Fig. 11(a) a similar discharge with RF injection results in an increase in the plasma duration by about 100 msec when an 80 msec long RF pulse with $P_{RF} \simeq$ 50 kW is injected into the device. The waves were launched in the direction of the ohmic electron drift (relative adjacent waveguide phasing of + 90°). In the present case the current enhancement is $\Delta I \simeq$ 50 kAmp at times t ≃ 200 msec into the discharge. The loop voltage at the plasma edge sharply decreases during RF injection to a value of less than 0.3 Volt whereas in the case without RF it is typically 1 Volt at t = 150 msec. The density during the application of the RF power was $\bar{n} \simeq$ (2-3) X 10^{13} cm^{-3}, but then decayed to lower values as the current was dying away beyond 300 msec into the discharge. These discharges were molybdenum dominated (limiter material) and are characterized by high Z_{eff} values and strong non-thermal $2\omega_{ce}$ emission and X-ray spectra, characteristic of the "slide-away" regime [13].

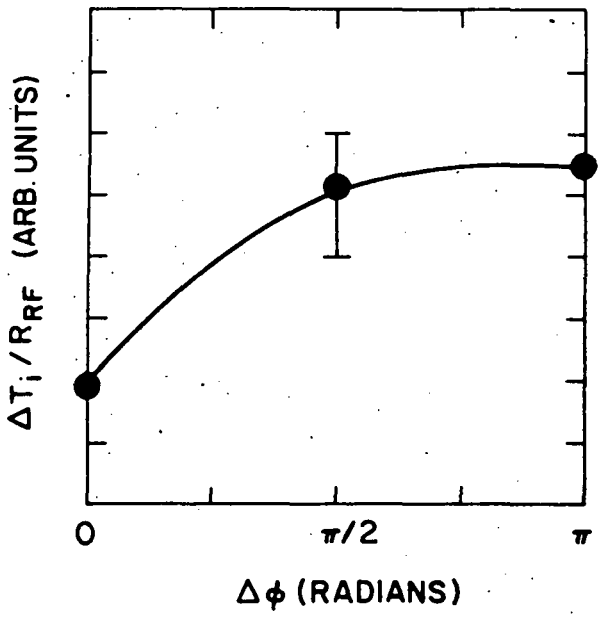

Fig. 13. ΔT_i, normalized to P_{RF}, vs. $\Delta\phi$, the relative phase between adjacent waveguides. $\bar{n}_e = 2.6 \times 10^{13}$ cm^{-3}, $B_o = 1.35$T.

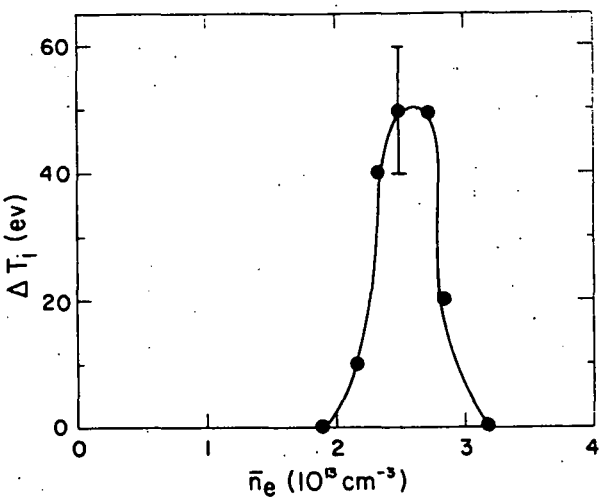

Fig. 14. T_i vs. $\bar{n}_e$, as obtained from the OVII lines. P_{RF} = 50 kW, B_o = 1.35T.

VERSATOR II EXPERIMENTS

1. RF Power and Antenna System

Lower hybrid heating studies at 800 MHz are being carried out on the Versator II research tokamak (R = 40 cm, a_L = 13 cm, $B_T \leq 1.5$ T) [14,15]. A four waveguide grill (height 24 cm, guide width 2.5 cm) is used in this experiment. For a phase difference $\Delta\phi = 180°$ between adjacent waveguides, the calculated Brambilla power spectrum is peaked at $N_{||} = 5.5$ and has a full width $\Delta N_{||} \simeq 3$ at half maximum. RF power, provided by a single 150 kW klystron is divided equally be waveguide splitters and fed into coaxial lines, each of which contains a phase shifter, directional coupler, and a ceramic vacuum window. The power is then coupled into the evacuated waveguide grill structure which extends approximately 1.5 m radially outward from the tokamak outer wall.

Prior to installation of the antenna on the tokamak the all-stainless steel grill was vacuum-baked at 350°C to outgas the waveguide surface so as to reduce the duration of the RF conditioning period required for high power operation. For the same reason, the grill is heated in situ to 150°C when not in use. Before beginning heating experiments each day, the grill is RF conditioned for approximately one hour with 100 kW of RF power. The grill is considered to be clean when no changes in the reflected phase and power are observed during the RF pulse at the power level to be used in the experiment. In addition, cyclotron breakdown in the evacuated waveguides during tokamak operation is suppressed with the application of an auxiliary vertical magnetic field over the grill region (see paper by Knowlton, Porkolab, and Luckhardt at this conference). No deleterious effect on plasma confinement has been noted as a result of the use of this additional magnetic field.

2. Experimental Results

Ion heating experiments to date have been performed with the following plasma parameters: toroidal field B_T = 1.35 T, plasma current I_p = 50-60 kA,

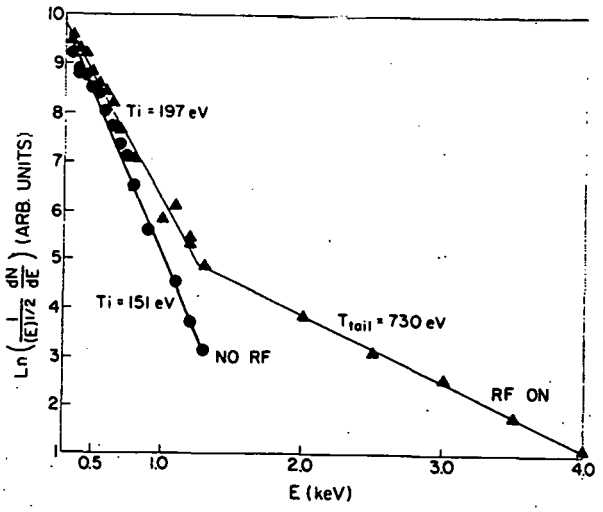

Fig. 15. Perpendicular charge exchange neutral spectrum with and without RF. Same parameters as in Fig. 12.

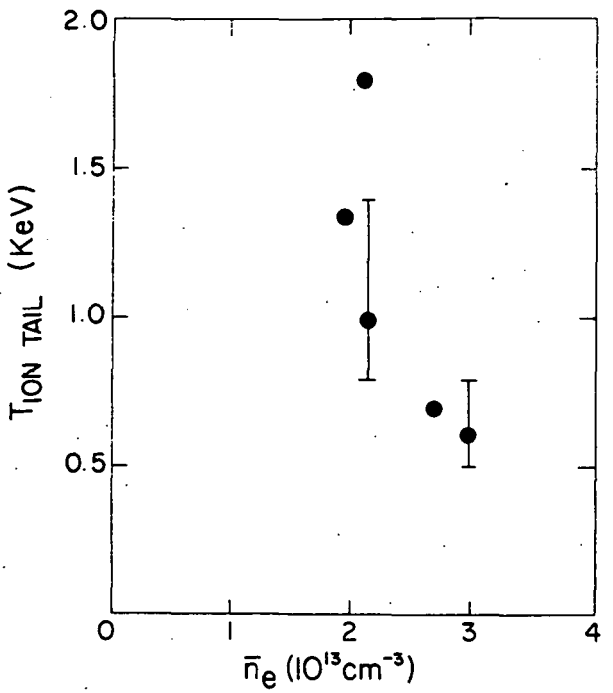

Fig. 16. Mean ion tail temperature, T_i(tail), deduced from charge exchange neutral spectrum vs. $\bar{n}_e$. B_o = 1.35 T.

loop voltage V_L = 2-2.5 V, line-averaged electron density $\bar{n}_e$ = 1.4-3 X 10^{13} cm^{-3}, central electron and ion temperature T_e = 400 eV and T_i = 120-150 eV, and effective ion charge Z_{eff} = 2.3. Hydrogen is the working gas. A portion of the tokamak wall is gettered prior to experimental runs. Good coupling (80-90%) of the RF to the plasma is achieved for a relative phase between waveguides $\Delta\phi \geq 90°$. The transmitted power in these experiments ranges from 50-75 kW.

A maximum ion temperature increase of 50 eV for 50 kW transmitted RF power is measured by Doppler broadening of the OVII and NVI VUV lines at a density of $\bar{n}_e$ = 2.6 X 10^{13} cm^{-3}. Similar temperature rise is observed by perpendicular charge exchange measurements. Typical results of VUV spectrometer measurements are shown in Fig. 12. No change in the loop voltage is noted during these experiments. The density usually decreases by about 10% during the RF pulse; during experimental runs, this effect is compensated for by increasing the gas puff rate during RF injection so as to keep the density approximately constant. In Fig. 13 we show the variation of ΔT_i versus relative phasing of adjacent waveguides. We see that nearly equal heating is obtained for $\Delta\phi = 0°$ and 90° at this density, while the heating efficiency for $\Delta\phi = 0°$ is low, in agreement with plasma-waveguide coupling theory.

The variation of the bulk ion temperature increase with density is shown in Fig. 14. At this RF power level, the heating band is narrow ($\bar{n}$ = (2.5 ± 0.5) X 10^{13} cm^{-3}) and is centered at a value of $f/f_{LH}(o)$ = 1.15 where f is the applied RF frequency of 800 MHz and $f_{LH}(o)$ is the central lower hybrid frequency, with the effect of impurities included (we assumed 5% O_2).

A perpendicular ion tail formed during the RF pulse, common to all lower hybrid heating experiments, is measured by charge exchange analysis to have a

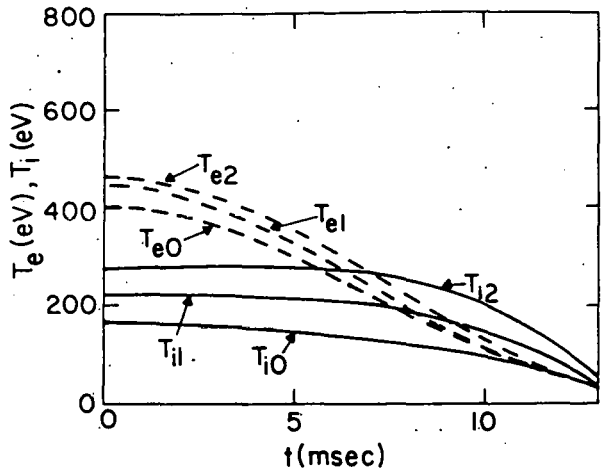

Fig. 17. Transport code modeling of RF heating in the Versator II tokamak. T_{io} and T_{eo} are the initial ion and electron temperature profiles. For T_{i1}, T_{e1} the edge temperatures are 20 eV, and for T_{i2}, T_{e2} the edge temperatures are 30 eV. $\bar{n}_e = 2.6 \times 10^{13}$, B = 13.5 kG, I = 55 kA.

temperature of 0.5-1.5 keV and a lifetime of 100 μsec or less. Figure 15 shows the charge exchange spectrum obtained in these experiments. We have not yet made a detailed study of this mean ion tail energy as a function of input power. While there is an apparent rise in the bulk temperature also (consistent with spectroscopic measurements) due to the large tail we cannot rely on this portion of the CX spectrum for accurate determination of the bulk ion temperature.

In Fig. 16 we show the mean ion tail energy ("tail temperature") as a function of density. We see that the tail "temperature" increases as the density decreases, and it exists to lower densities than the bulk ion heating (measured by the VUV spectrometer).

We have also made preliminary pyroelectric bolometric measurements of power lost to the wall. We find a 10-20 kW increase in the power lost to the wall during RF injection into the plasma. At present we have not yet made a detailed power balance during RF injection.

The bulk ion heating results obtained to date are not always reproducible. RF injection into plasmas with similar parameters during experimental runs on different days will not always give the same bulk ion temperature increase. Preliminary observations indicate that if the density decreases ($\Delta n/n \simeq 0.10$) as a result of RF injection, and if the density is in the proper range, the plasma is heated. If the density remains constant or increases when the RF power is injected, the ion temperature does not measurably increase. Large amounts of titanium-gettering are usually required to produce the density decrease during the RF pulse, and thus wall cleanliness and/or edge plasma conditions are likely to play a significant role in the RF power deposition during RF injection. Occasionally we failed to obtain bulk ion heating even when the RF power was injected into a clean gettered tokamak discharge so that no increase in impurity lines was noted. The only notable feature of such shots was a rise in the plasma density during the RF pulse.

It has been suggested that the electron temperature at the plasma edge plays a critical role in determining the heating efficiency [16]. The edge electron temperature determines the threshold levels for parametric instabilities which are believed to represent a loss mechanism for the incident RF power [17]. In this paper we shall suggest an alternate explanation, namely collisional damping of the lower hybrid waves at the plasma edge when toroidal ray propagation is also taken into account. Ray tracing and transport calculations for Versator II parameters indicate that efficient heating should

occur only if the electron temperature at the plasma edge (limiter) is at least 25-30 eV. For a 10 eV edge temperature the heating efficiency is degraded so that no bulk heating is expected to take place. These computer code predictions are shown in Fig. 17. Numerical code studies of the radial deposition profiles shown that electron absorption is due to collisional damping (outer half radius) and electron Landau damping (inner half radius) associated with toroidal ray propagation (which produces multi-pass absorption). The ion heating occurs in front of the lower hybrid mode conversion layer and is radially half-way out due to toroidal ray propagation effects.

Measurements made by a Langmuir probe located several mm behind the limiter indicate an electron temperature of 22-27 eV whether ion heating was observed or not. However, there may be differences in the temperature and density profiles inside the limiter, where heating is observed. Since the collisional damping rate varies as $(n/T_e)^{3/2}$, radial profile effects may be important. At present, we do not have a more definitive explanation for this irreproducibility of ion heating other than to note its relation to the behavior of the density during the RF pulse. Further attention will be paid to impurity behavior with regard to this problem. Parametric instabilities have also been observed in our experiments, but at present we do not have sufficient data to draw definitive conclusions regarding their effects upon the ion heating efficiency.

In summary, the ion temperature increases by up to 50 eV upon application of 50 kW RF power coupled to the plasma. The heating is observed over a narrow range of densities, and is dependent on the grill phasing. To date, heating has only been observed if the plasma density decreases slightly during the RF pulse. The power will be raised to the 100 kW level in the near future.

COMPUTATIONAL MODELING OF LHH OF TOKAMAKS

We have developed a computer model for lower hybrid heating of a tokamak plasma which incorporates a 1-D radial transport code and a toroidal ray tracing code. The details of this code are given in the paper by Luckhardt, et al. at this conference. The results of this code, as applied to the Alcator C and the Versator II regimes, were presented in Figs. 10, 11 and 17.

ACKNOWLEDGEMENTS

The Versator II 800 MHz RF power system was built at PPPL and is on loan from there. We thank Mr. R. Rohatgi for programming the computer, and Mr. S. McDermott for helping with setting up the CX diagnostic on Versator II. We also thank Mr. E. Fitzgerald and Mr. J. Nickerson on Versator II, and the entire operating crew of Alcator C for their expert technical assistance in operating the tokamaks.

This research was supported by the US Department of Energy Contract No. DE-AC02-78ET51013.

REFERENCES

[1] M. Porkolab, J. Schuss, Y. Takase, S. Knowlton, S. C. Luckhardt, et al., Proc. 8th Int. Conf. Plasma Phys. and Nucl. Fusion Res., Brussels, Belgium, 1980, IAEA-CN38/T-2-1, Vol. II, p. 507.

[2] J. Stevens, M. Ono, R. Horton, J. R. Wilson, Princeton University Plasma Physics Laboratory Report PPPL-1779, April 1981.

[3] J. J. Schuss, M. Porkolab, Y. Takase, S. Texter, Bull. Am. Phys. Soc. 26, 1023 (1981).

[4] R. Englade, et al., Proc. 2nd Joint Grenoble-Varenna Int. Symp., Como, Italy, September 1980 ("Heating in Toroidal Plasmas", EUR 7424EN, Vol. 1, p. 399). J. J. Schuss, MIT Plasma Fusion Center Report PFC/JA-82-1, December 1981.
[5] J. J. Schuss, M. Porkolab, Y. Takase, et al., Nucl. Fusion 21, 427 (1981).
[6] C. F. F. Karney, Phys. Fluids 22, 2188 (1979).
[7] Heating due to excitation of parametric instabilities in the center of the plasma is likely only if $\omega_o < 2\omega_{LH}$; see, for example, M. Porkolab, Phys. Fluids 20, 2058 (1977). M. Porkolab, S. Bernabei, W. M. Hooke, R. W. Motley, T. Nagashima, Phys. Rev. Lett. 38, 230 (1977).
[8] N. Fisch, Phys. Rev. Lett. 41, 873 (1978).
[9] T. Yamamoto, T. Imai, M. Shimada, et al., Phys. Rev. Lett. 45, 716 (1980).
[10] M. Nakamura, T. Cho, S. Kubo, et al., Phys. Rev. Lett. 47, 1902 (1981).
[11] S. C. Luckhardt, M. Porkolab, S. F. Knowlton, et al., Phys. Rev. Lett. 48, 152 (1982).
[12] W. Hooke, C. Barnes, S. Bernabei, et al., Bull. Am. Phys. Soc. 26, 975 (1981).
[13] A. A. M. Oomens, L. Th. M. Ornstein, R. R. Parker, F. C. Schuller, R. J. Taylor, Phys. Rev. Lett. 36, 255 (1976).
[14] S. Knowlton, K. I. Chen, S. C. Luckhardt, F. S. McDermott, M. Porkolab, Proc. 4th Topical Conf. on RF Plasma Heating, Austin, Texas, paper C11, February 1981.
[15] M. Porkolab, J. Schuss, Y. Takase, K. I. Chen, S. Knowlton, S. C. Luckhardt, S. McDermott, Proc. 2nd Joint Grenoble-Varenna Int. Symp., Como, Italy, September 1980 ("Heating in Toroidal Plasmas", EUR 7424EN, Vol. 1, p. 355).
[16] N. Suzuki, et al., Proc. 8th Int. Conf. on Plasma Phys. and Nucl. Fusion Res., Brussels, Belgium, 1980, Vol. II, p. 525.
[17] T. Imai, et al., Phys. Rev. Lett. 43, 586 (1979).

PFC BASE LIST

INTERNAL MAILINGS (MIT)

G. Bekefi
36-213

A. Bers
38-260

D. Cohn
NW16-250

B. Coppi
26-201

R.C. Davidson
NW16-202

T. Dupree
38-172

S. Foner
NW14-3117

J. Freidberg
38-160

A. Gondhalekar
NW16-278

M.O. Hoenig
NW16-176

M. Kazimi
NW12-209

L. Lidsky
38-174

E. Marmar
NW16-280

J. McCune
31-265

J. Meyer
24-208

D.B. Montgomery
NW16-140

J. Moses
NE43-514

D. Pappas
NW16-272

R.R. Parker
NW16-288

N.T. Pierce
NW16-186

P. Politzer
NW16-286

M. Porkolab
36-293

R. Post
NW21-

H. Praddaude
NW14-3101

D. Rose
24-210

J.C. Rose
NW16-189

R.M. Rose
4-132

B.B. Schwartz
NW14-5121

R.F. Post
NW21-203

L.D. Smullin
38-294

R. Temkin
NW16-254

N. Todreas
NW13-202

J.E.C. Williams
NW14-3210

P. Wolff
36-419

T.-F. Yang
NW16-164

Industrial Liaison Office
ATTN: Susan Shansky
Monthly List of Publications
39-513

MIT Libraries
Collection Development
ATTN: MIT Reports
14E-210

B. Colby
PFC Library
NW16-255

EXTERNAL MAILINGS

National

Argonne National Laboratory
Argonne, IL 60439
ATTN: Library Services Dept.

Battelle-Pacific Northwest Laboratory
P.O. Box 99
Richland, WA 99352
ATTN: Technical Information Center

Brookhaven National Laboratory
Upton, NY 11973
ATTN: Research Library

U.S. Dept. of Energy
Washington, D.C. 20545
ATTN: D.O.E. Library

Roger Derby
Oak Ridge National Lab.
ETF Design Center
Bldg. 9204-1
Oak Ridge, TN 37830

General Atomic Co.
P.O. Box 81608
San Diego, CA 92138
ATTN: Library

Lawrence Berkeley Laboratory
1 Cyclotron Rd.
Berkeley, CA 94720
ATTN: Library

Lawrence Livermore Laboratory
UCLA
P.O. Box 808
Livermore, CA 94550

Oak Ridge National Laboratory
Fusion Energy Div. Library
Bldg. 9201-2, ms/5
P.O. Box "Y"
Oak Ridge, TN 37830

Dr. D. Overskei
General Atomic Co.
P.O. Box 81608
San Diego, CA 92138

Princeton Plasma Physics Laboratory
Princeton University
P.O. Box 451
Princeton, NJ 08540
ATTN: Library

Plasma Dynamics Laboratory
Jonsson Engineering Center
Rensselaer Polytechnic Institute
Troy, NY 12181
ATTN: Ms. R. Reep

University of Wisconsin
Nuclear Engineering Dept.
1500 Johnson Drive
Madison, WI 53706
ATTN: UV Fusion Library

EXTERNAL MAILINGS

International

Professor M.H. Brennan
Willis Plasma Physics Dept.
School of Physics
University of Sydney
N.S.W. 2006, Australia

Division of Plasma Physics
Institute of Theoretical Physics
University of Innsbruck
A-6020 Innsbruck
Austria

c/o Physics Section
International Atomic Energy Agency
Wagramerstrasse 5
P.O. Box 100
A-1400 Vienna, Austria

Laboratoire de Physique des Plasmas
c/o H.W.H. Van Andel
Dept. de Physique
Universite de Montreal
C.P. 6128
Montreal, Que H3C 3J7
Canada

Plasma Physics Laboratory
Dept. of Physics
University of Saskatchewan
Saskatoon, Sask., Canada S7N OWO

The Library
Institute of Physics
Chinese Academy of Sciences
Beijing, China

Mrs. A. Wolff-Degives
Kernforschungsanlage Julich GmbH
Zentralbibliothek - Exchange Section
D-5170 Julich - Postfach 1913
Federal Republic of Germany

Preprint Library
Central Research Institute for Physics
H-1525 Budapest, P.O. Box 49
Hungary

Plasma Physics Dept.
Israel Atomic Energy Commission
Soreq Nuclear Research Center
Yavne 70600
Israel

The Librarian (Miss DePalo)
Associazione EURATOM - CNEN Fusione
C.P. 65-00044 Frascati (Rome)
Italy

Librarian
Research Information Center
Institute of Plasma Physics
Nagoya University
Nagoya, 464
Japan

Dr. A.J. Hazen
South African Atomic Energy Board
Private Bag X256
Pretoria 0001
South Africa